

LA-UR-16-21901

Approved for public release; distribution is unlimited.

Title: Investigation of Surface Phenomena in Shocked Tin in Converging

Geometry

Author(s): Rousculp, Christopher L.

Oro, David Michael Griego, Jeffrey Randall Turchi, Peter John Reinovsky, Robert Emil Bradley, Joseph Thomas III

Cheng, Baolian

Freeman, Matthew Stouten Patten, Austin Randall

Intended for: proton radiography PAC proposal

Issued: 2016-03-21



Investigation of Surface Phenomena in Shocked Tin in Converging Geometry

C.L. Rousculp, D.M. Oro, J.R. Griego, P.J. Turchi, R.E. Reinovsky, J.T. Bradley, B. Cheng, M.S. Freeman, A.R. Patten — 16 March 2016

Background

There is great interest in the behavior of the free surface of tin under shock loading. While it is known that meso-scale surface imperfections can seed the Richtmyer-Meshkov Instability (RMI) for a surface that is melted on release, much less is known about a tin surface that is solid, but plastically deforming. Here material properties such as shear and yield strength come into play especially in converging geometry.

Previous experiments have been driven by direct contact HE. Usually a thin, flat target coupon is fielded with various single-mode, sinusoidal, machined, profiles on the free surface. The free surface is adjacent to either vacuum or an inert receiver gas. Most of these previous driver/target configurations have been nominal planer geometry. With modern HE it has been straightforward to shock tin into melt on release. However it has been challenging to achieve a low enough pressure for solid state on release.

Here we propose to extend the existing base of knowledge to include the behavior of the free surface of tin in cylindrical converging geometry. By shock loading a cylindrical tin shell with a magnetically driven cylindrical liner impactor, the free surface evolution can be diagnosed with proton radiography. With the PHELIX capacitor bank, the drive can easily be varied to span the pressure range to achieve solid, mixed, and liquid states on release. A conceptual cylindrical liner and target is shown in Figure 1.

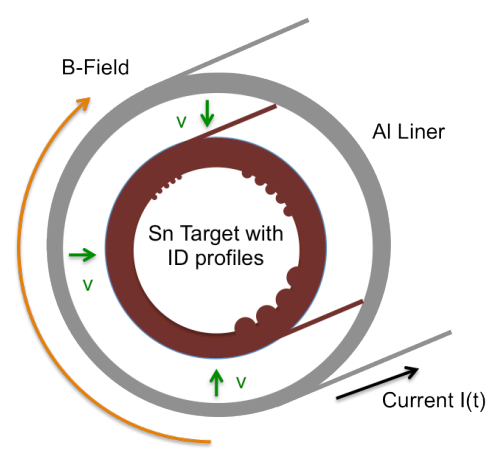


Figure 1. Conceptual cylindrical and target. The target has thee different single-mode flute profiles on the inner

Motivation

Current computational modeling paradigms of ejecta¹ are broken down into production, transport, and evolution. The production model is based on characteristic surface roughness and material phase. When a fluid, non-smooth surface is subject to shock, the RMI produces spikes of material that can be ejected from the surface. This model has been verified and quantified in an extensive series of experiments where single mode initial surface perturbations were subject to HE shock loading and melt on release ii,iii. Proton radiography imaged nonlinear amplitude growth and piezo pins measured total ejected mass as a function of time. However, one shortcoming of these HE driven experiments is that the drive is fixed and it is difficult to shock a tin sample such that it is solid on release. Thus a variable drive method that could span the range of pressures for release into solid, mixed, or fluid state would be highly valuable.

Recent theoretical work on the EOS of tin has modified both the Hugoniot and the isentropes for release into various states in tabular data. The new multiphase EOS for tin, SESAME 2161, includes the beta and gamma solid phases as well as a liquid phase. It predicts a lower pressure boundary for release to pure solid (~20 GPa) and a higher-pressure boundary for release to pure liquid (~35 GPa) than the existing SESAME 2160 table. Seen in Figure 2, is a phase space comparison of the two tables^{iv}. Experimentally, the new table requires a much broader range of accessible pressure drive to validate.

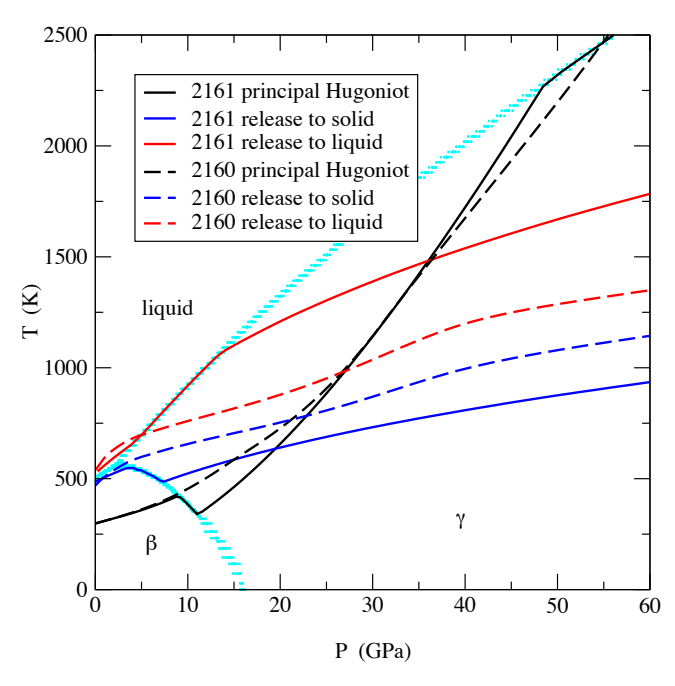


Figure 2. Phase diagram comparing multiphase SESAME 2161 with 2160.

Also under development in the ASC Lagrangian Applications Project (LAP) Flag code is a multi-phase material model that is phase-aware. There, a Steinberg-Guinan strength model is applied with separate parameters to the beta and gamma phases while the liquid phase is strengthless.^v

The main technique for the study of RMI growth and validation of models has been single-mode sinusoidal profile of a planer tin surface. However, if a similar profile is imposed on the inside of a cylinder, it is not as clear what the mechanism for amplitude growth might be when the cylinder is driven radially inward. On the one hand, if conservation of cylindrical solid area is assumed, then for constant velocity, amplitude growth can be shown to be proportional to $t^{1/2}$. However, if conservation of cylindrical fluid mass is assumed then the amplitude at early time grows linearly as

$$A(t) \approx A_0 (1 + \frac{vt}{R_0})$$

Here, R_0 is the initial cylinder radius; v is the surface's radial velocity. Note that it is independent of the mode number of the perturbation^{vi}

Magnetic Pulsed-Power Hydrodynamics

For these experiments the Precision High Energy-density Liner Implosion Experiment (PHELIX) portable capacitor bank will be utilize. PHELIX is a 300 kJ capacitor bank located at the LANL LANSCE proton radiography facility. It is capable of delivering a 4 MA, 10 us current pulse to a low inductance cylindrical load. A picture of PHELIX at pRad is shown in Figure 3.



Figure 3. PHELIX at pRad.

PHELIX was designed to achieve the same velocities and pressures as larger capacitor systems by scaling down in size liner-on-target experiments and requiring less stored energy^{vii}.

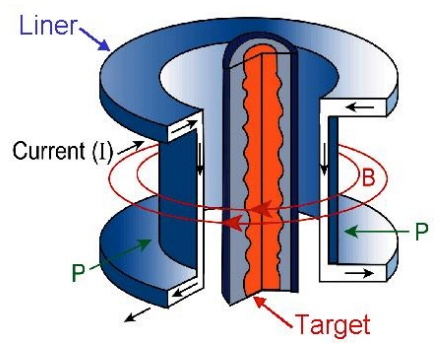


Figure 4. Schematic of a magnetically driven, liner-on-target experiment.

A general, magnetically driven, cylindrical liner-on-target, shock experiment is shown in Figure 4. For an axial directed current, *I*, passing through a liner of radius, *R*, an azimuthal directed magnetic field, *B*, produces a driving pressure given by,

$$P = \frac{\mu_0 I^2}{8\pi^2 R^2}$$

Thus, the same drive pressure can be achieved by keeping the ratio of *I/R* constant. By utilizing PHELIX with pRad (instead of traditional 4-frame flash X-ray imaging), a high-quality, high data rate can be achieved per experiment in an economical fashion.

Results of Crenulation-1

The first in this series of experiments was conducted in December of 2015. A 3 cm diameter Al liner and a 1 cm diameter tin target was fielded. For this experiment both the region between the liner/target and the region inside the target were evacuated to few mTorr. A cutaway view of the liner-on-target system is shown in Figure 5.

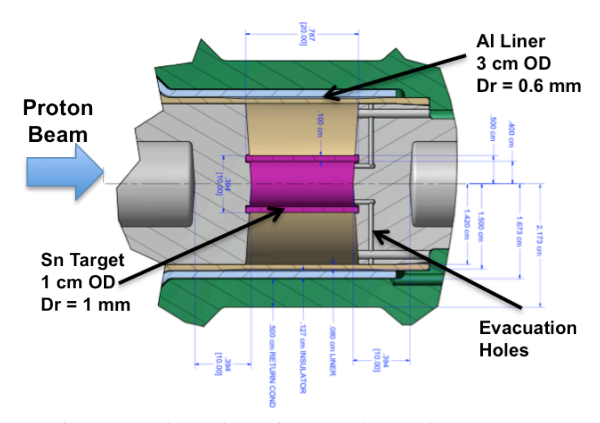


Figure 5. Cutaway view of the Crenulation-1 liner-on-target sytem.

The ID of the tin target was divided into three 120-degree sectors. Each sector had a single-mode perturbation of wavelength 1.10 mm machined into the surface with $\sim\!60$ -degrees of unperturbed surface between. The amplitude of the perturbation varied to give a wavelength/amplitude product, kA = 0.1, 0.2, and 0.3. A surface finish of 3.57/21.91 micro-in on the OD/ID of the target was achieved. Detail of the layout is shown in Figure 6.

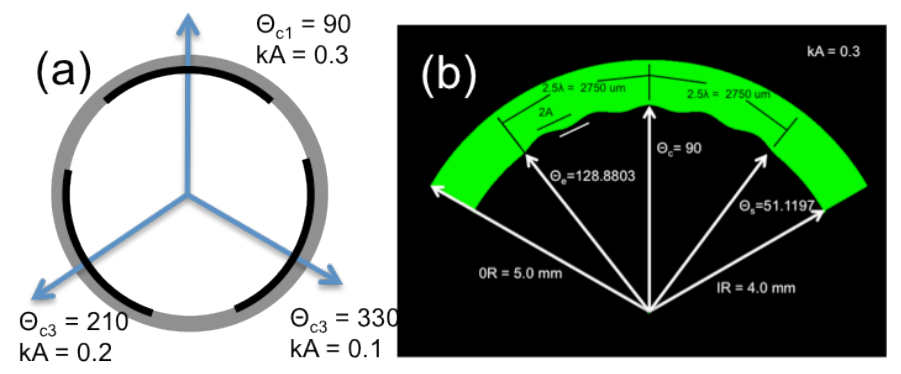


Figure 6. (a) Three sector layout of the ID of the tin target. (b) Details of the kA = 0.3 sector.

Optical Faraday rotation measured the drive conditions for Cren-1. The time profile of the current delivered to the load is shown on the left in Figure 7. It shows a peak current of 3 MA with a 10 us pulse. By modeling the liner-on-target system, the shock pressure in the tin target can be inferred. Shown on the left in Figure 7 is the shock profile in the tin. A peak pressure of 0.37 Mbar (37 GPa) is achieved for \sim 0.3 us followed by the release from the rarefaction from the ID. This shock is more than enough to achieve fully melt-on-release in tin. It should be noted that the slight drop (\sim 2 GPa) in pressure before release is due to the convergent geometry of the system.

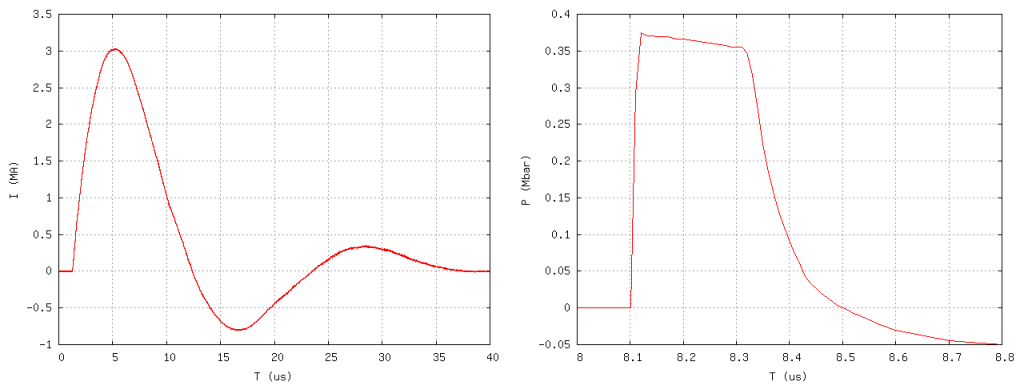
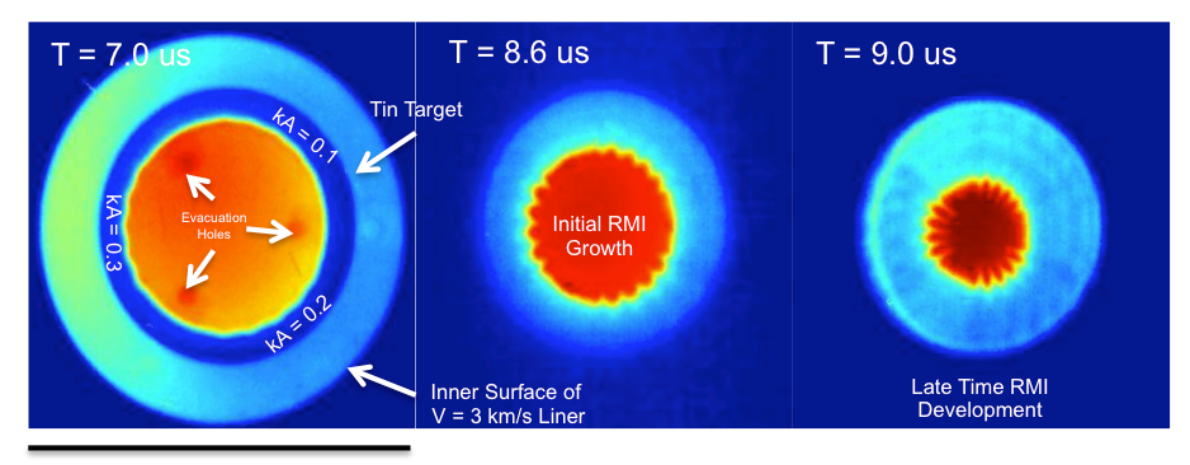


Figure 7. (Left) Measured load current for Cren-1. (Right) Shock pressure in the tin target.

A twenty-one-image pRad movie was captured during the experiment. A few sample images of the RMI growth from the three sectors are shown in Figure 8.



15 mm

Figure 8. Three sample pRad images from the Cren-1 experiment showing the evolution of three sectors of the single-mode perturbation.

The images have been analyzed and the growth of the kA = 0.3 sector has been compared to calculations. Figure 9 shows calculations and a comparison to the data. Good agreement is seen and the amplitude appears linear in time. This is consistent with the theory of conservation of shell volume. Also, it should be noted that in the calculation at late times, a density depression (cavitation) due layer is observed near the OD of the target. This is indicated by dark blue at T = 9.0 us in Figure 9. The structure is also seen in the data in Figure 8.

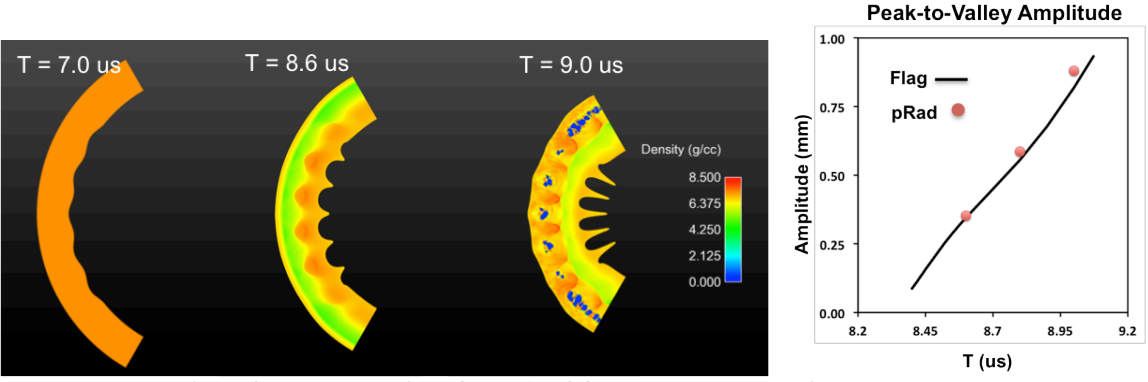


Figure 9. Flag calculation of the kA = 0.3 sector and a comparison to the data.

While the overall amplitude growth in time is linear, the velocities of tip of the spike and pit of the bubble display time-varying structure. A plot of velocity versus time is shown in Figure 10 for each of the different sectors. All display the same qualitative behavior with the same breakout velocity (v = 0.25 cm/us) and the spike and bubble profiles scaling with kA. The smooth surface is identical in all three cases. After shocking, the spike tip has a constant acceleration followed by gentle deceleration. Effectively, the tip is RMI accelerated as it transitions from a valley to a peak. It is then effectively free streaming. The bubble has an immediate deceleration caused by RMI followed by acceleration due to convergence finishing with a deceleration caused by a rarefaction from the OD. The smooth surface has slight acceleration as would be expected in a converging geometry system, followed by a deceleration due to the rarefaction from the OD.

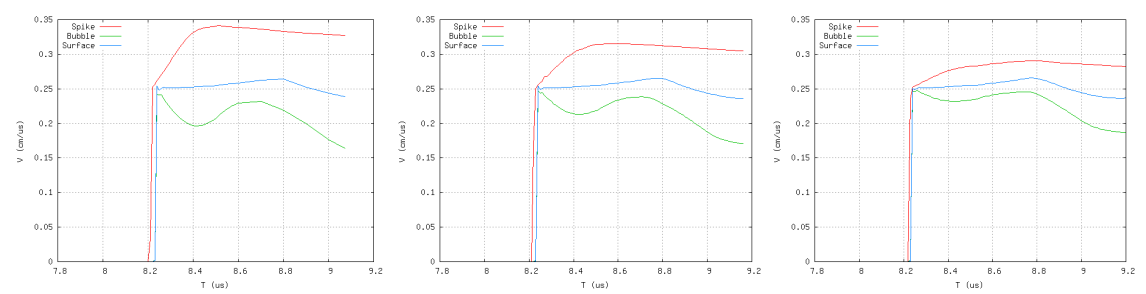
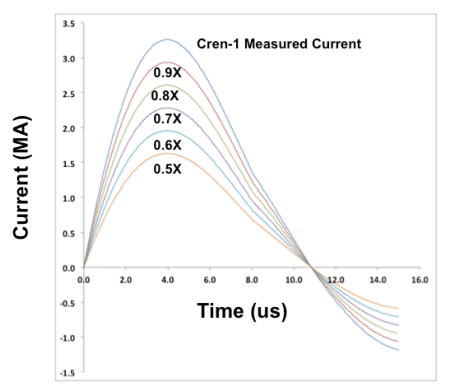


Figure 10. Velocity from calculation of spike, bubble, and smooth surface in time for kA = 0.3 (left), 0.2 (middle), and 0.1 (right).

Computational Study of Release to Mixed and Solid States

The proposed next experiment would shock an identical tin target into a solid or mixed state upon release. To study this, a series of calculations has been performed in which the measured current is fractionally scaled. This is a feature readily achievable by with pulsed power, but difficult with HE drive. Figure 11 shows both the scaled load current profiles used in simulations and the resulting liner velocity, shock velocity, and shock pressure.



| Scale | Liner Velocity | V_shock in Tin | P_shock in Tin |
|--------|----------------|----------------|----------------|
| Factor | (km/s) | (km/s) | (Gpa) |
| 1 | 2.9 | 1 | 38 |
| 0.9 | 2.1 | 0.9 | 29 |
| 0.8 | 1.5 | 0.8 | 20 |
| 0.7 | 1.3 | 0.65 | 14 |
| 0.6 | 1 | 0.4 | 9.5 |
| 0.5 | 0.74 | 0.3 | 7.3 |

Figure 11. (Left) Fractional scaling of the load current used in simulations. (Right) Drive parameter from the simulations.

I = 0.8x Case

The 0.8x case is interesting for two reasons. First, as the spikes release into the liquid phase, but at late time the tips refreeze into the beta phase where strength traps the advancing liquid and causes blunting of the tip. Second, the bubbles release to solid, but under compression from convergence end up in the liquid state and develop a secondary structure. The calculation is shown in Figure 12 with the left being colored by density and the right being colored by dominant phase in a cell. Finally, the velocities of the spike and bubble show that the spike profile is the same as in the I = 1.0x case, the bubble actually experiences a strong acceleration under convergence and had a greater velocity than then spike when the calculation terminates due to mesh tangling. The velocity profiles are shown in Figure 13. It should be kept in mind that that while the model includes multiphase EOS and phase aware strength; it does not include surface tension.

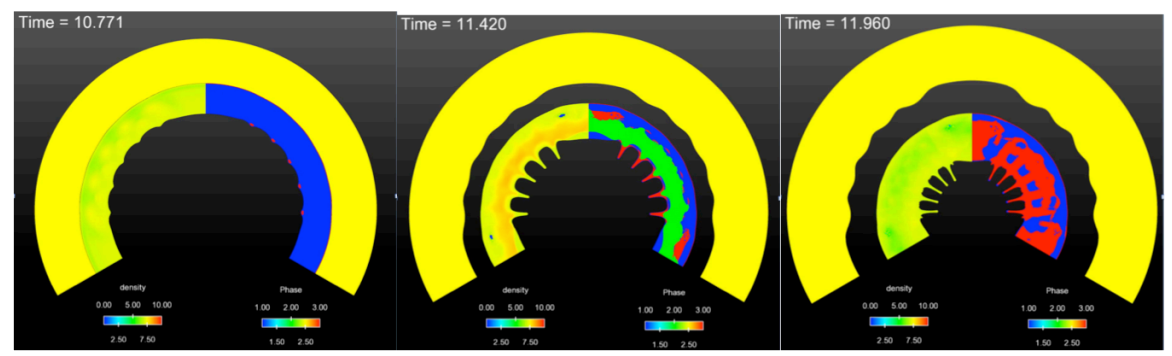


Figure 12. I = 0.8X, kA = 0.3 simulation. Spike release to liquid (red) but have their tips refreeze into the beta phase (blue) causing blunting at late time. The bulk transitions from beta to gamma (green) and liquid.

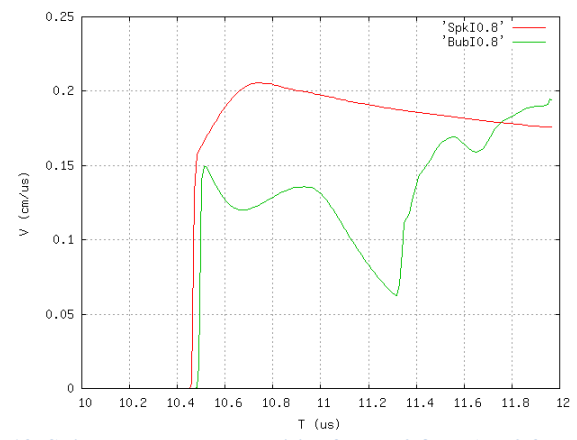


Figure 13. Spike and bubble velocities for I = 0.8x, kA = 0.3 calculation.

I = 0.6x Case

By reducing the drive even further, the tin target can be made to remain in the beta phase throughout the implosion. The single-mode perturbation still inverts under RMI, but the amplitude growth is suppressed by material strength. Shown in Figure 14 are the initial and final states of the single-mode perturbation in the calculation.

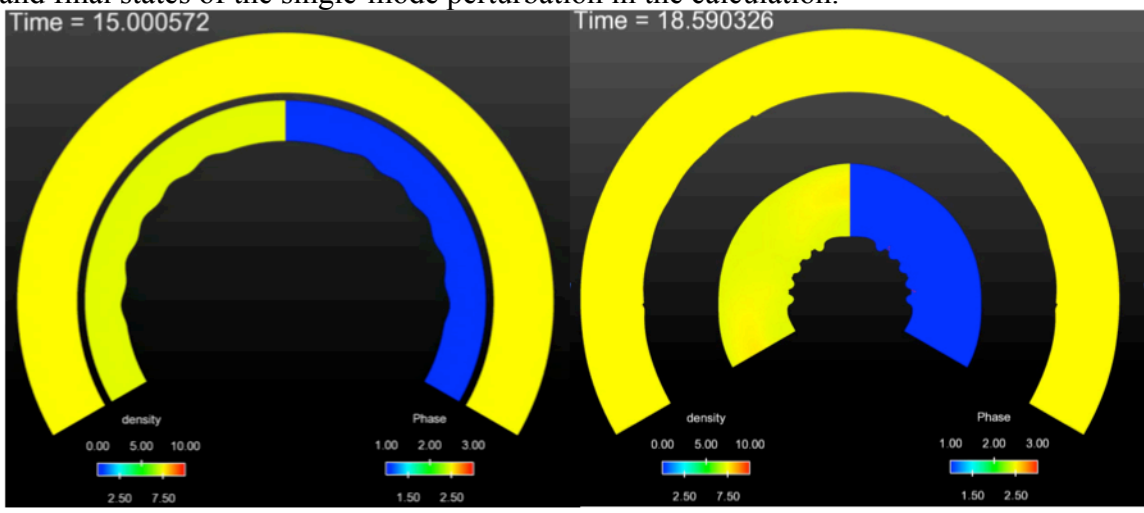


Figure 14. I = 0.6x, kA = 0.3 calculation before impact and when the calculation terminates.

Looking at the velocities of the spike and bubble in Figure 15, the transit time reflections of shocks between the inner and outer surfaces becomes apparent. This causes the

interesting effect of the bubble moving faster than the spike, which means the amplitude is shrinking under convergence. This leads to the question that if a shell of the same thickness but with an initially larger radius, were driven at the same shock pressure, would the perturbation amplitude go to zero?

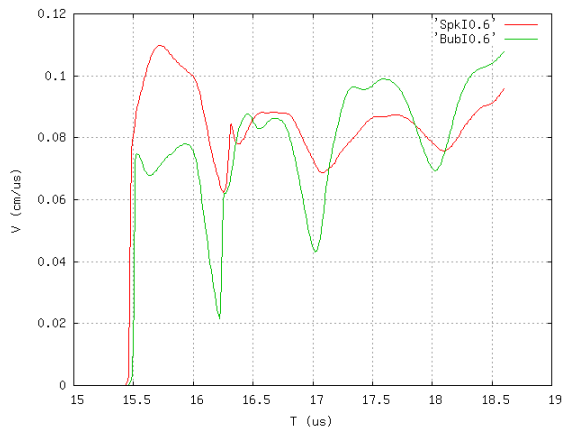


Figure 15. Spike and bubble velocity profiles for the I = 0.6x, kA = 0.3 case. Note at late time the bubble velocity is greater than the spike.

Experimental Requirements

The previous computational study leads to proposal of two experiments in the upcoming beam cycle:

- 1. Shock to release in a mixed state with the drive current approximating the I = 0.8x case. The main feature of interest would be the shapes of the spikes at late times.
- 2. Shock to release in a solid state with the drive current approximating the I = 0.6x case. The main feature of interest would be the inversion of the single mode perturbation and the eventual decrease in the spike-to-bubble amplitude.

Requirements for both experiments:

- PHELIX driver and load current diagnostics
- A week of pRad time after maintenance week
- Currently one target is fabricated and assembled. A second experiment would require fabrication and assembly of a second.
- The 7X Magnifier with 21 images. Since maximum spatial resolution is required. Qualification of the new magnifier would be ideal.

Follow on Experiments

Because of the flexibility of the PHELIX driver and the pRad diagnostics several follow-on experiments are envisioned. These include:

- PDV of Spike and Bubble
- Gas Fill
- Non-Orthogonal Shock
- Non-Sinusoidal Perturbation

i J. Fung, et al., "Ejecta Modeling in the FLAG Hydrocode," LA-UR-08-3835.
ii W. T. Buttler and M. B. Zellner, "Tin Ejecta Data Review: Toward a Statistical Material Fragmentation Model." LA-UR-07-6522.
iii W. T. Buttler et al., "Unstable Richtmyer-Meshkov Growth of Solid and Liquid Metals

in Vacuum," J. Fluid Mech., 703, 60-84, 2012.

iv C. Greef, E. Chisolm, D. George, "SESAME 2161: An Explicit Multiphase Equation of State for Tin," LA-UR-05-9414.

^v T. Canfield and T. Carney, private communication.

vi L. G. Margolin and M. J. Andrews, "Models for Crenulation of a Converging Shell," Transactions of the ASME, **136**, 084501-4, 2014.

vii P. J. Turchi, IEEE-TPS 34, 1919-1927, 2006.